Journal of Renewable Materials

Tech Science Press

DOI: 10.32604/jrm.2022.022594

ARTICLE

Controlled-Release of Plant Volatiles: New Composite Materials of Porous Carbon-Citral and Their Fungicidal Activity against *Exobasidium vexans*

Yaoguo Liu[1], Yao Chen[2], Huifang Liu[2], Wei Chen[1], Zhiwei Lei[2], Chiyu Ma[2], Jie Yin[1] and Wen Yang[2,*]

[1]College of Tea Science, Guizhou University, Guiyang, 550025, China

[2]Guizhou Tea Research Institute, Guizhou Academy of Agricultural Sciences, Guiyang, 550006, China

[*]Corresponding Author: Wen Yang. Email: yangwen3409@126.com

Received: 16 March 2022 Accepted: 12 May 2022

ABSTRACT

Citral (Eo) exhibits excellent fungicidal activities. However, it is difficult to maintain long-term fungicidal activity due to its strong volatility. Herein, a controlled-release strategy by using biomass-derived porous carbon (BC) was developed to overcome the drawback of Eo. New composite materials were prepared by loading Eo on tea stem porous carbon (BC@Eo), and their controlled-release fungicidal activity against *Exobasidium vexans* was assessed. BC with a large specific surface area of 1001.6 m^2/g and mesoporous structure was fabricated through carbonization temperature of 700°C. The BC@Eo materials were characterized using Fourier-transform infrared spectroscopy and X-ray powder diffraction. The results suggested that chemical and physical interactions occurred in BC@Eo. The Eo release profile suggested a biphasic pattern with an initial fast release on days 1–14 and a subsequent controlled phase on days 14–30. The *in vitro* cumulative release percentage of Eo from BC@Eo was 51% during one month, and this result was significantly lower than that from free Eo (cumulative release percentage of Eo of 82% in one week). The antifungal activities of Eo and BC@Eo against *E. vexans* were determined using the inhibition zone method. The results indicated that Eo and BC@Eo formed large inhibition zones of 19.66 ± 0.79 and 21.92 ± 0.77 mm, respectively. The influence on the hyphal structure of *E. vexans* was observed by scanning electron microscopy on day 30. The hyphal structure of *E. vexans* treated with BC@Eo was more shrunken than that treated with Eo at 30 days, suggesting that BC@Eo prolongs the fungicidal activity against E. vexans. This study demonstrated that the encapsulation of Eo in BC for developing the BC@Eo materials could be a promising strategy to inhibit volatility and maintain the fungicidal activity of Eo and provide a potential alternative for the reuse of abundant tea biomass waste resources.

KEYWORDS

Exobasidium vexans; porous carbon; citral; controlled release; fungicidal activity

Nomenclature

Eo	Citral
XRD	The X-ray powder diffraction
FTIR	Fourier-transform infrared spectroscopy
S_{BET}	The BET surface areas
SEM	Scanning electron microscope
TGA	Thermogravimetric analysis

1 Introduction

The development of green, environmentally friendly, safe, and efficient natural fungicides to replace chemical fungicides is urgently needed to control plant disease. Essential oils are one of the candidates to be used as fungicides [1–5]. Citral (Eo), the active ingredient in many plants' essential oils, exhibits appreciable and extensive *in vitro* antimicrobial activity against bacteria and fungi [6–10]. Eo has been allowed by the European Commission as a flavoring ingredient in food (Regulation EU 872/2012), approved for application by the Food and Drug Administration, and recognized as a safe ingredient for use as a food additive and human consumption (GRAS 182.60) [11]. However, Eo is volatile, sensitive to light and heat, and is prone to oxidative decomposition [8]. These factors limit their exploitation in the practical application fields.

Improving the stability and durability of essential oils and their monomer components in practical applications is a key research issue. A considerable number of composite materials have been reported to maintain biological activity, inhibit volatility, and increase the effective utilization rate [12]. It has been reported that mesoporous silica with an ultra-high specific surface area of 1036.5 m^2/g was used as a carrier for cinnamaldehyde [13]. Mesoporous composites of microcrystalline cellulose and zeolitic imidazole frameworks with a surface area of 236.2 m^2/g were used for the temperature-controlled release of essential oils [14]. These composites are characterized by abundant pore structure and high specific surface area. Biomass-derived porous carbon materials were often used as adsorbents, supercapacitors, catalysts, fuel cells, batteries, etc., because of their abundant pore structure and high specific surface area [15–19]. However, few studies on biomass-derived porous carbon as a carrier for essential oils have been reported.

Tea is one of the three major non-alcoholic beverages globally and the main economic crop in developing countries like China, India, and Kenya. Because of its high economic value, the tea planting area was rapidly expanding in China [20]. In 2017, the tea planting area was about 3.05 million hectares in China [21]. Tea stem waste biomass is 14,175–60,210 kg/ha [22]. Overall, tea production results in more than 50% of tea stem waste. Hence, abundant tea stem wastes are the ideal biomass resources to produce porous carbon.

Tea blister blight disease caused by *Exobasidium vexans* is the most serious foliar disease affecting tea in Asia. This disease causes about 60% of crop loss and adversely affects the quality of tea products [23,24]. This disease attains epidemic proportions during monsoon months and virtually disappears during the drier months [25–28]. *E. vexans* is a highly pathogenic basidiomycete spread by wind-borne basidiospores [29–32]. Fungicides, i.e., carbendazim, hexaconazole, propiconazole, and trienmorpholine have been used to control tea blister blight disease through existing methods. These fungicides are used every two weeks in the disease's prevalent period to prevent the blister blight fungus in tea plantations. However, this measure comes with considerable additional financial costs and pesticide residue problems [33–36]. Thus, natural fungicides to replace chemical fungicides are urgently needed to control this disease.

This study aims to inhibit volatility and maintain the biological activity of Eo using new composite materials, which were derived from the biological wastes of tea stem resources. The resulting materials were characterized using Fourier-transform infrared spectroscopy and X-ray powder diffraction (BC@Eo). In addition, their controlled-release properties and fungicidal activity against *E. vexans* were assessed.

2 Materials and Methods

2.1 Materials

Tea stem was obtained from the Zunyi Meitan Tea plantation (Guizhou, China), and citral (CAS 5392–40–5, 95% HPLC purity) was from Yuanye Biotechnology Co., Ltd. (Shanghai, China). KOH(CAS 1310–58–3, 85%) and HCl (CAS 7647–01–0, 37%) were purchased from Aladdin Chemical Reagent Co., Ltd. (Shanghai, China). All chemicals were of analytical reagent grade and Ultrapure water (18 MΩ/cm) was

used throughout the experiment. *E. vexans* (tea blister blight) was obtained from Guizhou Tea Research Institute, Guizhou Academy of Agricultural Sciences, Guiyang, Guizhou, China.

2.2 Synthesis of BC and BC@Eo

The tea stems were crushed and heated directly to 300°C for 4 h at a heating rate of 5°C min^{-1} in the presence of a nitrogen atmosphere. The precarbonized biochar was mixed with KOH, and the impregnation ratio of KOH/precarbonized biochar was 4:1. The samples were heated to 600°C, 700°C, and 800°C for 1.5 h at a heating rate of 5 °C min^{-1}, respectively. After activation, the obtained material was ground and adjusted to pH 7 with 0.1 M HCl and Ultrapure water, and finally dried at 85°C overnight. The obtained tea stem porous carbon samples were stored for further use. The three porous carbon materials were immersed in Eo at room temperature for 24 h to prepare the controlled-release system. The swollen weights of the Eo-loaded porous carbon materials were obtained by gently removing the surface Eo. The loading rate (SI) was then calculated using Eq. (1):

$$SI(\%) = \frac{BC@Eo - BC}{BC} \times 100\% \tag{1}$$

2.3 Characterization of BC and BC@Eo

The X-ray powder diffraction (XRD, Smartlab 9, Japan) patterns of tea stem, C−700 (BC), and BC@Eo were obtained through the Philips X'pert diffractometer. The functional groups of BC and BC@Eo were obtained by Fourier transform infrared spectrometer (FTIR, Thermo Scientific Nicolet-6700, USA). BC and BC@Eo structures were observed by scanning electron microscopy (SEM, Hitachi SU8220, Japan). The BET surface areas (S_{BET}) of BC were obtained by analysis of isothermal nitrogen adsorption/desorption date (Tristar 3000, Micromeritics).

2.4 Thermal Stability Study

The thermal stability of pure Eo and BC@Eo were evaluated by Thermogravimetric Analysis (TGA; Q50, TA, USA). Pure Eo (10 mg) and BC@Eo (10 mg) were placed in a TGA furnace and heated from 30°C to 600°C at a heating rate of 10 °C min^{-1} under a nitrogen atmosphere.

2.5 In Vitro Release Studies

The *in vitro* release study of pure Eo and BC@Eo was carried out in an open space. Pure Eo and BC@Eo were placed in an open space at room temperature (12,000–14,000 KDa). The total Eo cumulative amounts from pure Eo and BC@Eo were estimated through UV–vis spectrophotometry (Cary 50, Varian, USA) at 229 nm. The cumulative release percentage of Eo represented by the ratio of the cumulative amount (M_t) of Eo released at each time interval to the initial amount (M_0) of the Eo encapsulated in the BC is illustrated in the following Eq. (2):

$$\text{Cumulative release percentage} = \sum\nolimits_{t=0}^{t} \frac{M_t}{M_0} \times 100\% \tag{2}$$

2.6 Determination of Fungicidal Activity against E. Vexans

The fungicidal activity of BC@Eo against *E. vexans* was determined using the disc diffusion method. An aliquot comprising 100 μL of 10^7 CFU/mL fungal suspension was spread onto the surface of PDA plates, and 1.67 mg BC@Eo, 1 mg Eo, and 0.67 mg BC were added to the surface of the agar. 3–5 parallel samples were prepared for each raw material and incubated for 72 h at 25°C. The diameters of the growth inhibition zones around the filter sheets were measured for semiquantitative evaluation. *E. vexans* was fumigated with 10 mg Eo and 16.7 mg BC@Eo. The influence on the hyphal structure of *E. vexans* after incubation for 7 and 30 days at 25°C was observed by SEM (Hitachi SU8220, Japan).

2.7 Statistical Analysis

All experiments were conducted thrice. Results were expressed as mean ± standard deviation. The SPSS software was utilized for statistical analysis. A one-way analysis of variance determined differences among the means, and $p < 0.05$ was considered statistically significant.

3 Results and Discussion

3.1 Selection of Optimal Porous Materials

N^2 adsorption/desorption tests were used to investigate porous carbon materials' surface area and pore size distribution to obtain the best materials for Eo loading. Precarbonized tea stem samples were further activated with KOH at temperatures of 600°C, 700°C, and 800°C, resulting in three porous materials labeled as C-600, C-700, and C-800, respectively. The S_{BET} values of C-600, C-700, and C-800 (Fig. 1A) were 592.8, 1001.6, and 670.5 $m^2 \cdot g^{-1}$, respectively. The corresponding surface areas increased remarkably, with the activation temperature rising from 600°C to 700°C. However, when the activation temperature rose from 600°C to 700°C, the corresponding surface area decreased. This phenomenon indicates that part of the material's pore structure will be lost at high temperatures [37,38].

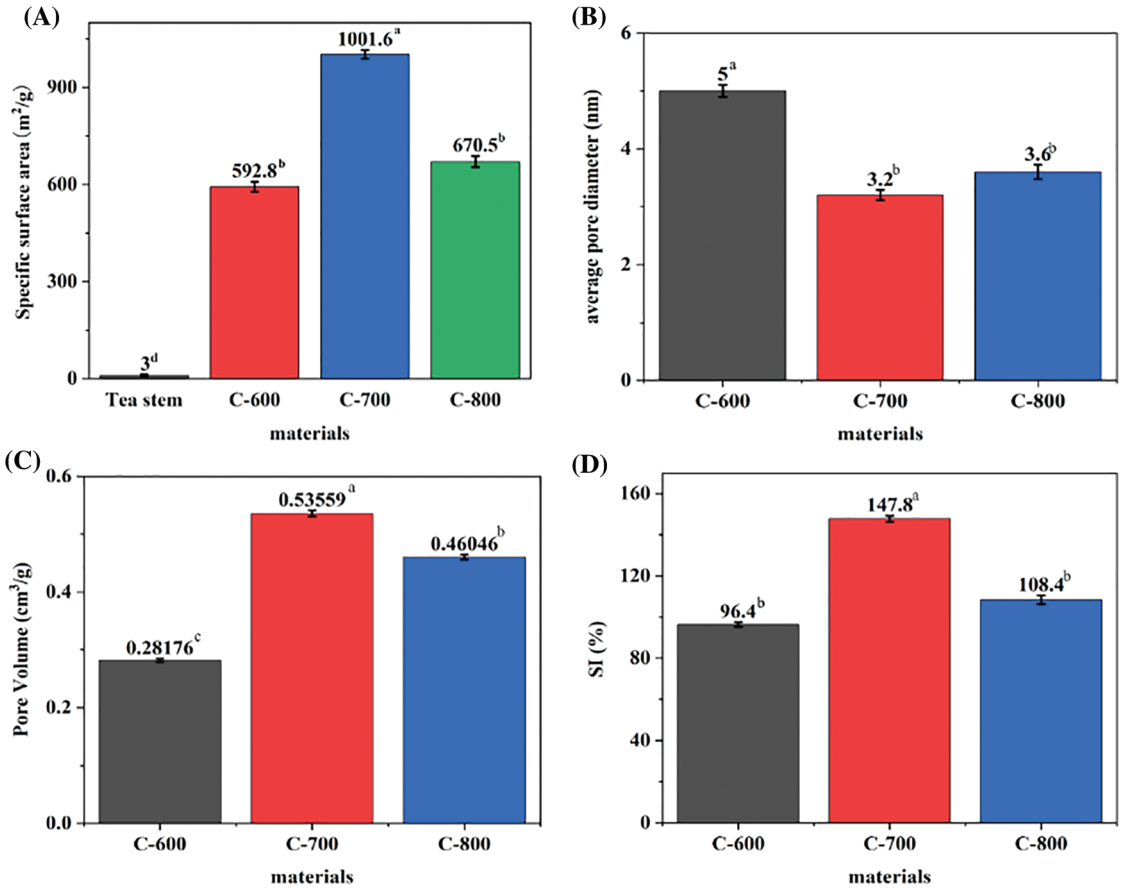

Figure 1: (A) BET specific surface areas of tea stem, C-600, C-700, and C-800, (B) Average pore diameter of the different activation temperatures, (C) Pore volume of the different activation temperatures, (D) SI of the different activation temperatures.

Note: Values labeled with a different letter (a–d) are statistically significantly different ($p < 0.05$), Error bars represent standard deviations.

To investigate the relationship between pore structure and load capability by analyzing the mesoporous size distribution and adsorption/desorption isotherms. The pore size distributions of C-600, C-700, and C-800 are shown in Figs. 2B–2D. Each material was found with narrow peaks with high intensity at 0.5–1 nm. Peaks became low and wide at high activation temperatures, indicating a loss of mesoporous structure. Adsorption/desorption isotherms are shown in Fig. 2A. According to the IUPAC classification, all isotherms were Type IV. A sharp increase in the low-relative pressure region revealed the existence of mesoporous [39]. Combined with the texture parameters in Fig. 1B, the activated samples can be classified as mesoporous materials.

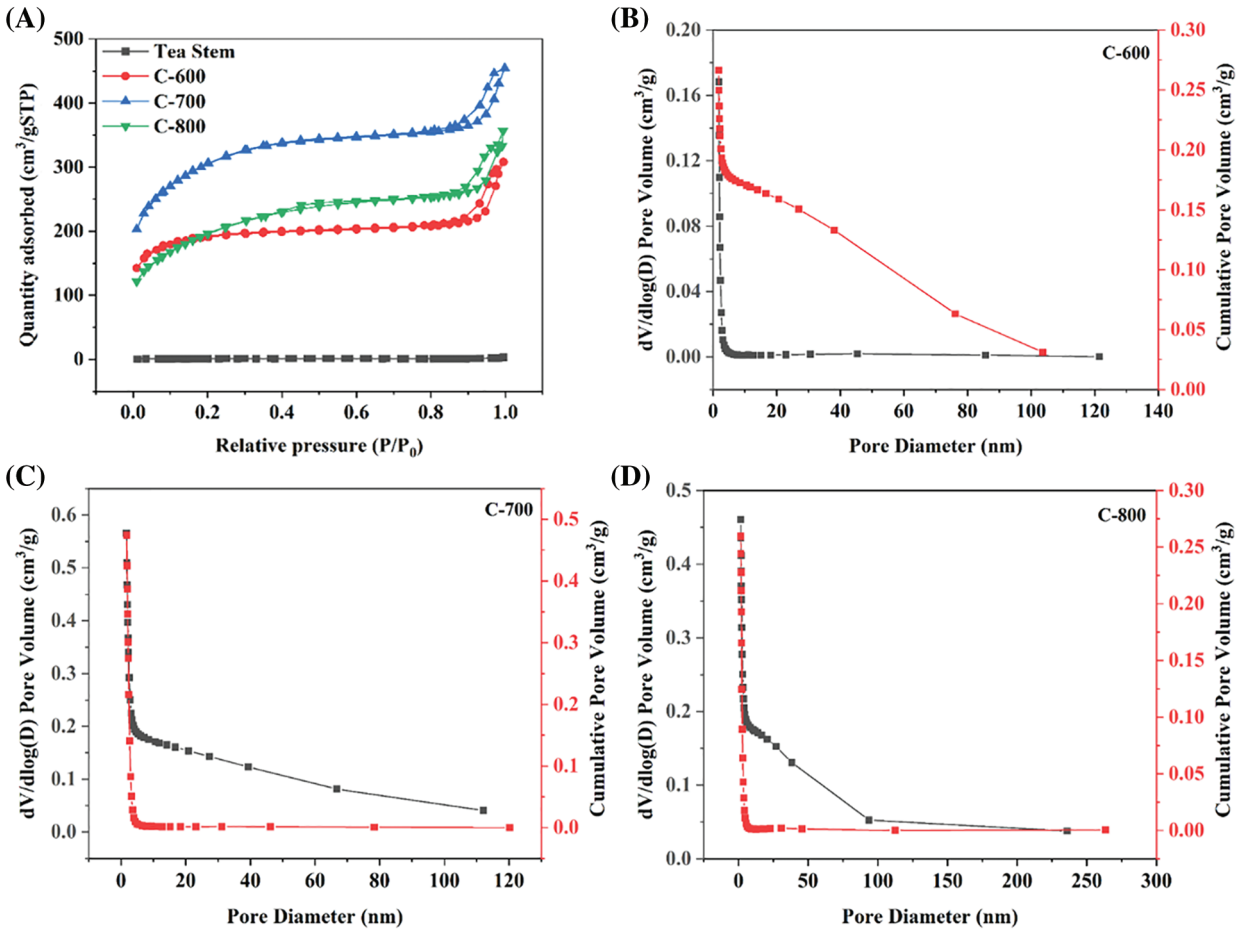

Figure 2: (A) Nitrogen adsorption/desorption isotherms of C-600, C-700, C-800, and tea stem (B–D) Pore size distributions of C-600, C-700, and C-800 by the BJH method

The Pore volume and surface area show the same trend, with the material activated at 700°C having the most significant pore volume (Fig. 1C). The phenomenon could be explained by the slow reaction between carbon and KOH, thus developing minimal pore volume at 600°C. The rapid reaction of carbon with KOH at a high temperature of 800°C leads to transforming micropores into mesopores, thereby reducing the pore volume and surface area.

The SI values of C-600, C-700, and C-800 (Fig. 1D) were 96.4%, 147.8%, and 108.3%, respectively. The corresponding SI increased remarkably when the surface area was raised. C-700 had the largest SI.

The morphologies of activated carbonized tea stem porous carbons C-600, C-700, and C-800 were characterized by SEM (Fig. 3). These three porous carbons exhibit high surface roughness with nanoscale features. Through the pore openings on the surface can access observe the inner pores of the three porous carbons. The SEM images of the three porous carbons show rich-developed surface pore structures, suggesting a honeycomb-like structure.

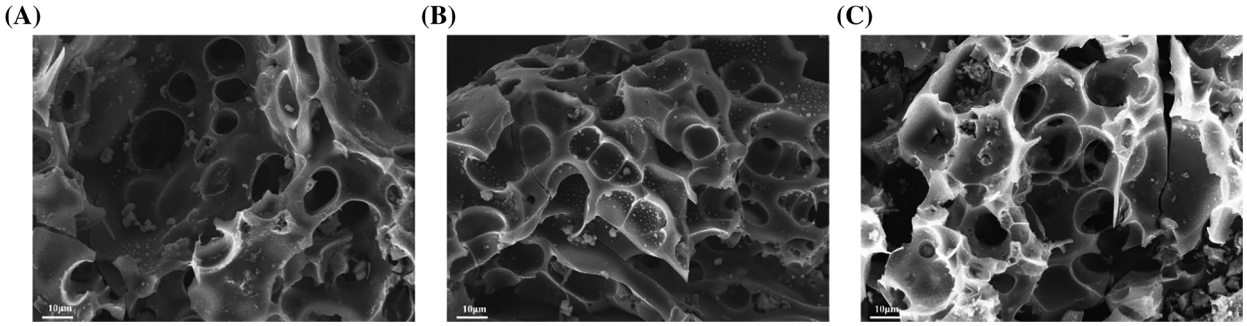

Figure 3: (A) SEM of C-600, (B) SEM of C-700, (C) SEM of C-800

Results showed that C-700(BC) had the largest S_{BET}, pore-volume, and SI and was chosen as the loading material for Eo.

3.2 Characterization of Tea Stem, BC, and BC@Eo

The XRD patterns of tea stem and BC are shown in Fig. 4A. The tea stems had a broad peak of crystalline character at $2\theta = 20°$. This crystalline characteristic peak in the XRD pattern of BC disappeared after pre-carbonization and activation. The results suggest that precarbonization and activation might destroy the crystalline structure in the tea stem. Therefore, BC contained predominantly amorphous components. Fig. 2A shows the nitrogen adsorption/desorption isotherms of tea stem and BC. The isotherm of BC was Type IV [40], indicating that BC was mesoporous materials, whereas untreated tea stems could be considered nonporous. According to N^2 adsorption/desorption data, the S_{BET} values of BC and tea stem were 1001.6 and 3 $m^2 \cdot g^{-1}$ (Fig. 1A). Results showed that precarbonization and activation contributed to increasing the surface area of BC. With BC's carbon molecules depleted and gases, including CO, H_2, and CO_2, were generated, leading the pores in the BC to be constantly generated and expanded in this process [41–43]. 0.1 M HCl solution and ultrapure water wash the surfaced soluble potassium salt away, leaving rich pores. Fig. 2C shows the pore size distributions of BC. Results indicated that BC contained mesopores (2–6 nm). For the BC@Eo complex, the incorporation of Eo led to a significant increase in the intensity of the BC's peak at 20.28° [44], which was due to the complexation of BC with Eo.

FTIR spectroscopy determined the surface functional groups of tea stem, BC, and BC@Eo. Results are shown in Fig. 4B. The principal spectral features of the tea stem were as follows: 3025 (O–H stretching superimposed on N-H stretching and inter-and extra molecular hydrogen bonds of the polysaccharide), 1713 (amide I band and C=O stretching), 1555 (NH_2 bending), 1458 (amide III band and C–N stretching), 1396 and 1344 (C–H bending), 1287 (C–N stretching), and 1188 (C–O stretching) cm^{-1} [45,46]. Compared with tea stem, the FTIR spectral peak intensity of BC at 1458 cm^{-1} decreased. This result indicated that the pre-carbonization and activation might lead to the C–N bond of the amide on BC being broken. The disappearance of BC peaks at 3025 cm^{-1} could be attributed to a fracture in the O–H bond. BC peaks at 1713, 1555, 1396, and 1188 cm^{-1}, disappeared, which might be because the bridge C=O, NH_2, C–H, C–O bonds were almost destroyed. Hence, the FTIR spectra of tea stem porous carbon

materials demonstrated that the surface groups of the original tea stem were remarkably altered. The surface morphologies of tea stem porous carbon materials are shown in Fig. 3 and the information for sizes and structures of tea stem porous carbon materials was provided. Many pores formed in the interior of tea stem porous carbon materials after activation. The pore diameter distribution in BC is shown in Fig. 2c. Countless small-diameter pores inside the wall of large-diameter channels. Therefore, the obtained BC has many pores, which contribute to the significant surface area of the BC. Compared with BC, BC@Eo was observed with the appearance of peaks at 3019 and 2943 cm^{-1}, which could be attributed to the integration of the C–H bond. BC peaks at 1689 (amide I band, C–O stretch), 1620 (NH_2 bending), 1400 (amide III bandstand, C–N stretch), and 1198 (bridge C–O–C stretch) cm^{-1} appeared. Therefore, BC was successfully loaded with Eo. All results demonstrated that a chemical interaction occurred in BC@Eo and not only physical blending.

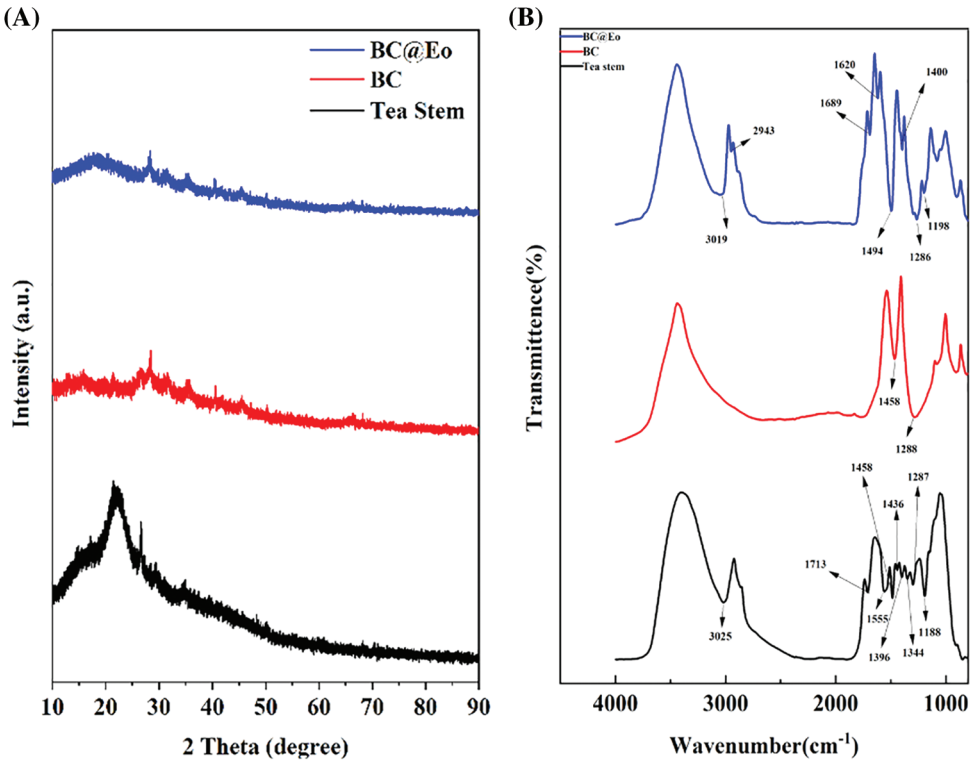

Figure 4: (A) XRD patterns of tea stem, BC and BC@Eo; (B) FTIR spectrum of tea stem, BC and BC@Eo

3.3 Thermal Stability of Eo and BC@Eo

The thermal stability of Eo and BC@Eo was investigated by TGA under a nitrogen atmosphere. As shown in Fig. 5, pure Eo had a significant weight loss between 100°C–200°C. The entire decomposition of BC@Eo displayed a pattern of two-step weight loss in the temperature range of 100°C–600°C. The first weight loss corresponded to 100°C–290°C, which could be explained by the loss of Eo in BC. The slow step degradation between 290°C and 600°C was attributed to BC. Compared with that of pure Eo, the degradation temperature of BC@Eo shifted to a high temperature (200°C–290°C), and the trend for BC@Eo was evidently slow due to the presence of Eo encapsulated in BC. This result indicated that Eo had thermal stability in the protection of BC. Compared with that of pure Eo, the increment of thermal stability of BC@Eo might be attributed to the following reasons. The honeycomb structure of BC

prolonged the pathway for Eo to evaporate, and strong inter-and intramolecular bonds appeared between Eo and BC.

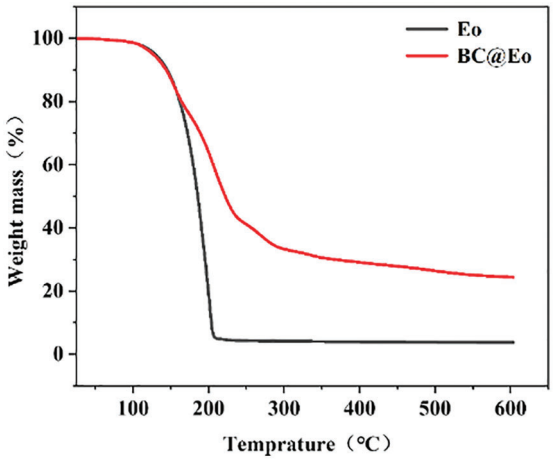

Figure 5: TGA analysis of Eo and BC@Eo

3.4 In Vitro Release Studies of Eo and BC@Eo

The release behavior of Eo and BC@Eo was evaluated. At room temperature, the cumulative release amount of Eo in the controlled-release system of BC@Eo was persistent and slow. In the first week, the BC@Eo release amounts increased significantly and continued to increase slightly, and only 51% of Eo in BC@Eo was released in one month (Fig. 6). The cumulative release amounts of pure Eo decreased markedly with prolonged time compared with those from BC@Eo (cumulative release amounts reached 82% after one week). This decrease in the cumulative release of Eo from BC@Eo could be due to the compact structure formed by BC and Eo. Compared with that from pure Eo, the release of Eo from BC@Eo was divided into two stages based on the release rate of BC@Eo. The rapid release in the first stage was to release the Eo on the outer surface of BC, and the rich pore structure of BC caused the slow release of the second stage. This phenomenon made the surface area of Eo coming in contact with air small, thereby resulting in slow release.

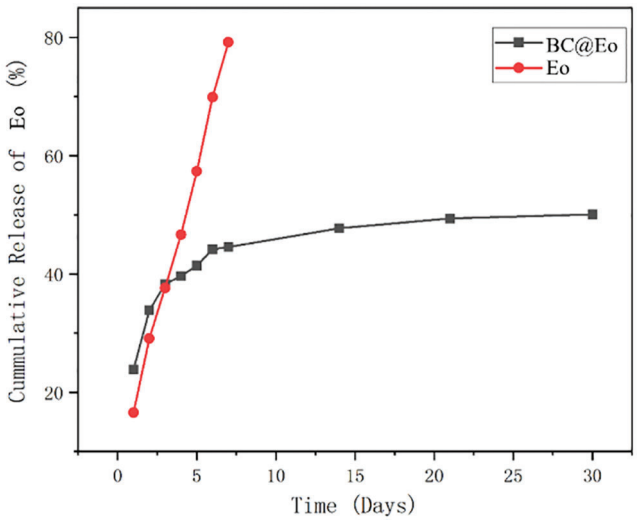

Figure 6: Release of BC@Eo and Eo

3.5 Fungicidal Activity Analysis

The fungicidal activities of BC, BC@Eo, and pure Eo were investigated to evaluate the fungicidal efficiencies of free Eo and BC@Eo and determine whether the inhibitory effect of Eo could be enhanced by the controlled-release system. As shown in Fig. 7 and Table 1, BC, BC@Eo, and Eo exhibited different fungicidal activities against *E. vexans* with inhibition zones of 0.00, 21.92 ± 0.77, and 19.66 ± 0.79 mm, respectively. BC had no fungicidal activity against *E. vexans*. For pure Eo, the surface of the mycelium became shriveled after fumigation to cultivate for initial 7 days (Figs. 8A and 8B) because the hydrophobicity of Eo enabled them to interact with fungus cell membranes, thus making them permeable [11]. Subsequently, the degree of shrinkage of the surface of the hyphae had little change on days 7–30 (Fig. 8C). This finding might be because of the overconsumption and decomposition of Eo by light [1–3]. Nevertheless, the fungicidal activity of BC@Eo continuously increased in the experimental time range with increasing time. The folds of the mycelium during the 30-day treatment were more significant than those of the 7-day treatment. This finding might be attributed to Eo's slow and controlled release from BC@Eo (Figs. 8D and 8E). Therefore, the fungicidal efficacy of BC@Eo was higher than that of pure Eo in a long incubation period. This finding might be attributed to Eo's slow and controlled release from BC@Eo. This slow-release strategy will be more green, environmentally friendly, and safe compared with existing methods.

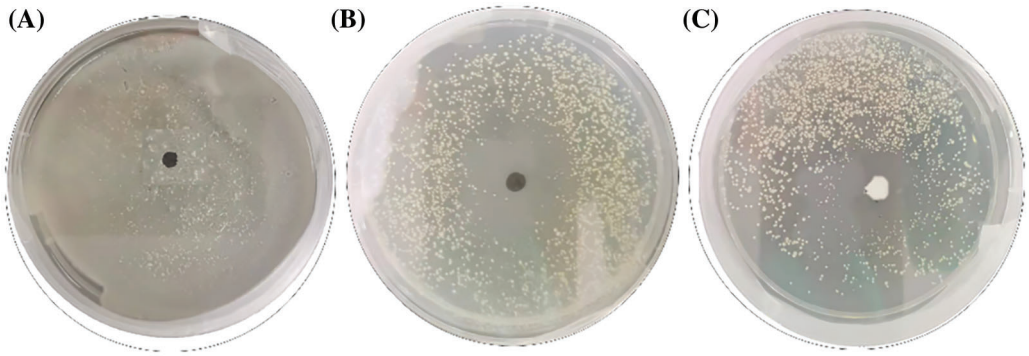

Figure 7: (A) The inhibition zone of BC; (B) The inhibition zone of BC@Eo; (C) The inhibition zone of pure Eo

Table 1: The inhibition zone of BC, BC@Eo, and pure Eo

Samples	Inhibition zone diameter (mm)
BC	0.00^{b}
BC@Eo	21.92 ± 0.77^{a}
Eo	19.66 ± 0.79^{a}
Sterile water	0.00^{b}

Note: a and b manifest significantly different ($p < 0.05$) according to the Duncan test.

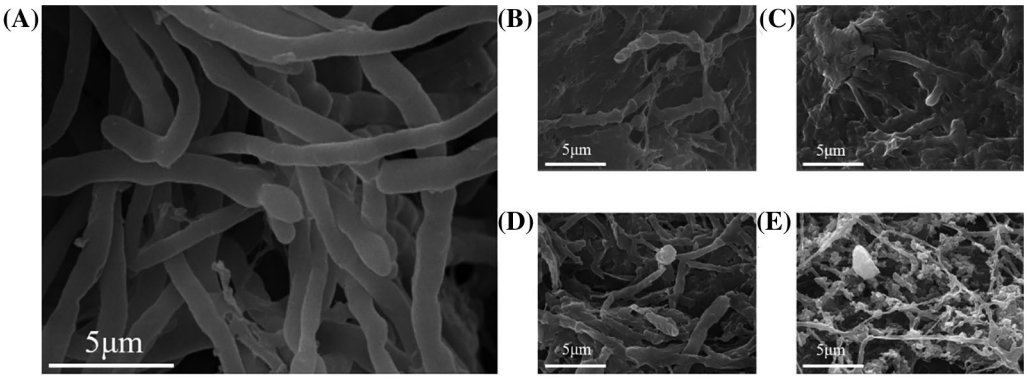

Figure 8: (A) The SEM of *E. vexans*; (B and C) The SEM of *E. vexans* were treated with Eo for 7 and 30 days, respectively; (D and E) The SEM of *E. vexans* were treated with BC@Eo for 7 and 30 days, respectively

4 Conclusions

A novel controlled-release materials of BC@Eo were developed to improve the fungicidal activity of Eo against *E. vexans*. Tea stem waste was used to produce porous carbon materials with a large specific surface area of 1001.6 m^2/g and mesoporous structure, which could become carriers for a controlled-release system. According to the measurements from the released amount of Eo in BC@Eo and pure Eo within 30 days, BC@Eo had a desirable controlled release effect for Eo. The results of the *in vitro* bioassay showed that BC@Eo and pure Eo had an excellent inhibition effect against *E. vexans*. In contrast, the porous carbon materials did not show fungicidal activity, indicating that Eo was the active ingredient in the controlled-release system. According to the effect of BC@Eo and pure Eo on *E. vexans* hyphal structure at 30 days, the results indicated that BC@Eo prolonged the duration of Eo against *E. vexans*. These results indicated that the encapsulation of Eo in BC for the production of BC@Eo with the controlled-release properties could efficiently enhance the fungicidal activity of Eo by reducing its volatilization. Meanwhile, this porous carbon provides a new environmentally friendly way to reuse tea production waste. This controlled-release strategy may be extended to other botanical pesticides to possess a longer duration and a better fungicidal activity.

Acknowledgement: We thank National-Regional Joint Engineering Research Center for Soil Pollution Control and Remediation in South China, Guangdong Key Laboratory of Integrated Agro-Environmental Pollution Control and Management, Institute of Eco-Environmental and Soil Sciences, Guangdong Academy of Sciences for providing space and support during the experiments. We thank J. H. Cui for his guidance and software suggestions in data processing.

Funding Statement: This work was funded by the Ministry of Finance and Ministry of Agriculture and Rural Affairs: Supported by National Modern Agricultural Industry Technology System, Youth Science and Technology Fund of Guizhou Academy of Agricultural Sciences No. [2020]02, Guiding Project of Guizhou Academy of Agricultural Sciences No. [2018]01.

Conflicts of Interest: The authors declare that they have no conflicts of interest to report regarding the present study

References

1. Amiri, A., Mottaghipisheh, J., Jamshidi-Kia, F., Saeidi, K., Vitalini, S. et al. (2020). Antimicorbial potency of major functional foods'essential oils in liquid and vapor phases: A short review. *Applied Sciences, 10,* 8103. DOI 10.3390/app10228103.

2. Guimarães, A. C., Meireles, L. M., Lemos, M. F., Guimarães, M. C. C., Endringer, D. C. et al. (2019). Antibacterial activity of terpenes and terpenoids present in essential oils. *Molecules, 24,* 2471. DOI 10.3390/molecules24132471.
3. Huang, K., Liu, R., Zhang, Y., Guan, X. (2021). Characteristics of two cedarwood essential oil emulsions and their antioxidant and antibacterial activities. *Food Chemistry, 346,* 128970. DOI 10.1016/j.foodchem.2020.128970.
4. He, F., Wang, W., Wu, M., Fang, Y., Wang, S. et al. (2020). Antioxidant and antibacterial activities of essential oil from atractylodes lancea rhizomes. *Industrial Crops and Products, 153,* 112552. DOI 10.1016/j.indcrop.2020.112552.
5. Hu, W., Li, C., Dai, J., Cui, H., Lin, L. (2019). Antibacterial activity and mechanism of litsea cubeba essential oil against methicillin-resistant staphylococcus aureus (MRSA). *Industrial Crops and Products, 130,* 34–41. DOI 10.1016/j.indcrop.2018.12.078.
6. Zhang, J., Du, C., Li, Q., Hu, A., Peng, R. et al. (2021). Inhibition mechanism and antibacterial activity of natural antibacterial agent citral on bamboo mould and its anti-mildew effect on bamboo. *Royal Society Open Science, 8,* 202244. DOI 10.1098/rsos.202244.
7. Thielmann, J., Muranyi, P. (2019). Review on the chemical composition of litsea cubeba essential oils and the bioactivity of its major constituents citral and limonene. *Journal of Essential Oil Research, 31,* 361–378. DOI 10.1080/10412905.2019.1611671.
8. Choudhary, G., Walia, S., Kumar, J., Kumar, B., Parmar, B. S. (2007). Synthesis and antifungal activity of citral oxime esters against two phytopathogenic fungi rhizoctonia solani and sclerotium rolfsii. *Pesticide Research Journal, 19,* 15–19.
9. Chueca, B., Pérez-Sáez, E., Pagán, R., García-Gonzalo, D. (2017). Global transcriptional response of escherichia coli MG1655 cells exposed to the oxygenated monoterpenes citral and carvacrol. *International Journal of Food Microbiology, 257,* 49–57. DOI 10.1016/j.ijfoodmicro.2017.06.002.
10. Qian, W., Liu, M., Fu, Y., Wang, T., Zhang, J. et al. (2020). Antimicrobial and antibiofilm activities of citral against carbapenem-resistant enterobacter cloacae. *Foodborne Pathogens and Disease, 17,* 459–465. DOI 10.1089/fpd.2019.2751.
11. Cao, J., Liu, H., Wang, Y., He, X., Jiang, H. et al. (2021). Antimicrobial and antivirulence efficacies of citral against foodborne pathogen vibrio parahaemolyticus RIMD2210633. *Food Control, 120,* 107507. DOI 10.1016/j.foodcont.2020.107507.
12. Marze, S. (2015). Bioaccessibility of lipophilic micro-constituents from a lipid emulsion. *Food & Function, 6,* 3218–3227. DOI 10.1039/c5fo00441a.
13. Guo, W., Wang, X., Huang, J., Cai, W., Wang, J. et al. (2020). Preparation and antimicrobial effect of a cinnamaldehyde-based sustained release fumigant tablet for grain storage. *Journal of Materials Research and Technology, 9,* 14122–14130. DOI 10.1016/j.jmrt.2020.09.130.
14. Abdelhameed, R. M., Alzahrani, E., Shaltout, A. A., Emam, H. E. (2021). Temperature-controlled-release of essential oil via reusable mesoporous composite of microcrystalline cellulose and zeolitic imidazole frameworks. *Journal of Industrial and Engineering Chemistry, 94,* 134–144. DOI 10.1016/j.jiec.2020.10.025.
15. Bi, Z., Kong, Q., Cao, Y., Sun, G., Su, F. et al. (2019). Biomass-derived porous carbon materials with different dimensions for supercapacitor electrodes: A review. *Journal of Materials Chemistry A, 7,* 16028–16045. DOI 10.1039/c9ta04436a.
16. Singh, G., Lakhi, K. S., Sil, S., Bhosale, S. V., Kim, I. et al. (2019). Biomass derived porous carbon for CO_2 capture. *Carbon, 148,* 164–186. DOI 10.1016/j.carbon.2019.03.050.
17. Cao, W., Zhang, E., Wang, J., Liu, Z., Ge, J. et al. (2019). Potato derived biomass porous carbon as anode for potassium ion batteries. *Electrochim Acta, 293,* 364–370. DOI 10.1016/j.electacta.2018.10.036.
18. Kaur, P., Verma, G., Sekhon, S. S. (2019). Biomass derived hierarchical porous carbon materials as oxygen reduction reaction electrocatalysts in fuel cells. *Progress in Materials Science, 102,* 1–71. DOI 10.1016/j.pmatsci.2018.12.002.
19. Matsaga, R. B. M., Yang, R., Dutta, S., Ok, Y. S., Wu, K. C. (2021). Recent progress in the development of biomass-derived nitrogen-doped porous carbon. *Journal of Materials Chemistry A, 9,* 3703–3728. DOI 10.1039/d0ta09706c.

20. Su, S., Zhou, X., Wan, C., Li, Y., Kong, W. (2016). Land use changes to cash crop plantations: Crop types, multilevel determinants and policy implications. *Land Use Policy, 50,* 379–389. DOI 10.1016/j.landusepol.2015.10.003.
21. Ni, K., Shi, Y., Yi, X., Zhang, Q., Fang, L. et al. (2018). Effects of long-term nitrogen application on soil acidification and solution chemistry of a tea plantation in China. *Agriculture*. *Ecosystems & Environment, 252,* 74–82. DOI 10.1016/j.agee.2017.10.004.
22. Singha, D. M. (2016). *Studies on litter production decomposition and nutrient recycling in tea agro ecosystem of Cachar district*. *Southern Assam (Ph.D. Thesis)*. Department of ecology and environmental science. Assam University, India.
23. Radhakrishnan, B., Baby, U. I. (2004). Economic threshold level for blister blight of tea. *Indian Phytopath, 57,* 195–196.
24. Gulati, A., Gulati, A., Ravindranath, S. D., Gupta, A. K. (1999). Variation in chemical composition and quality of tea (*Camellia sinensis*) with increasing blister blight (*Exobasidium vexans*) severity. *Mycological Research, 103,* 1380–1384. DOI 10.1017/S0953756299008941.
25. Ajay, D., Balamurugan, A., Baby, U. I. (2009). Survival of *Exobasidium vexans*, the incitant of blister blight disease of tea, during offseason. *International Journal of Applied, 4,* 115–123.
26. Shanmuganathan, N., Arulpragasam, P. V. (1966). Epidemiology of tea blister blight (*Exobasidium vexans*): II. The diurnal and seasonal periodicity of spores in the air over a tea estate. *Transactions of the British Mycological Society, 49,* 215–219. DOI 10.1016/S0007-1536(66)80056-6.
27. de Weille, G. A. (1960). Blister blight (*Exobasidium vexans*) in tea and its relationship with environmental conditions. *Netherlands Journal of Agricultural Science, 8,* 183–210. DOI 10.18174/njas.v8i3.17647.
28. Sinniah, G. D., Kumara, K. W., Karunajeewa, D., Ranatunga, M. (2016). Development of an assessment key and techniques for field screening of tea (*Camellia sinensis* L.) cultivars for resistance to blister blight. *Crop Protection, 79,* 143–149. DOI 10.1016/j.cropro.2015.10.017.
29. Punyasiri, P. A., Abeysinghe, I. S. B., Kumar, V. (2005). Preformed and induced chemical resistance of tea leaf against *Exobasidium vexans* infection. *Journal of Chemical Ecology, 31,* 1315–1324. DOI 10.1007/s10886-005-5288-z.
30. Chaliha, C., Kalita, E. (2020). Blister blight disease of tea: An enigma. In: *Diagnostics of plant diseases*. DOI 10.5772/intechopen.95362.
31. Zhao, X. Z., Wang, Y., Ren, Y. F., Li, D. X., Chen, Z. (2020). The morphology observation of infection process for the pathogen *Exobasidium vexans* of tea blister blight against tea leaf. *Chinese Agricultural Science Bulletin, 34,* 117–122. DOI 10.11924/j.issn.1000-6850.casb17020003.
32. Mohktar, N., Nagao, H. (2019). Histological description of *Exobasidium vexans* infection on tea leaves (*Camellia sinensis*). *Songklanakarin Journal of Science & Technology, 41*, 1021–1028.
33. Sen, S., Rai, M., Das, D., Chandra, S., Acharya, K. (2020). Blister blight a threatened problem in tea industry: A review. *Journal of King Saud University-Science, 32,* 3265–3272. DOI 10.1016/j.jksus.2020.09.008.
34. Chakruno, P., Banik, S., Sumi, K. (2021). Important diseases of tea (*Camellia sinensis* L.) and their integrated management. In: *Diseases of horticultural crops*, pp. 119–138. USA: Apple Academic Press.
35. Mabbett, T. (2016). Epidemiology and management of *Exobasidium vexans* (blister blight disease) on camellia sinensis (tea). *International Pest Control, 58,* 114.
36. Thakur, B. R., Masand, S. (2015). Efficacy of Nativo 75 WG against blister blight in tea [*Camellia sinensis* (L.) *O. Kuntze]*. *Himachal Journal of Agricultural Research, 41,* 86–88.
37. Inguanzo, M., Menendez, J. A., Fuente, E., Pis, J. J. (2001). Reactivity of pyrolyzed sewage sludge in air and CO_2. *Journal of Analytical and Applied Pyrolysis, 58,* 943–954. DOI 10.1016/S0165-2370(00)00143-1.
38. Bagreev, A., Bashkova, S., Locke, D. C., Bandosz, T. J. (2001). Sewage sludge-derived materials as efficient adsorbents for removal of hydrogen sulfide. *Environmental Science & Technology, 35,* 1537–1543. DOI 10.1021/es001678h.
39. Chiang, H., Chao, C., Chang, C. Y., Wang, C. F., Chiang, P. C. (2001). Residue characteristics and pore development of petrochemical industry sludge pyrolysis. *Water Research, 35,* 4331–4338. DOI 10.1016/S0043-1354(01)00159-2.

40. Sheindorf, C. H., Rebhun, M., Sheintuch, M. (1981). A Freundlich-type multicomponent isotherm. *Journal of Colloid and Interface Science, 79,* 136–142. DOI 10.1016/0021-9797(81)90056-4.
41. Lillo-Ródenas, M. A., Cazorla-Amorós, D., Linares-Solano, A. (2003). Understanding chemical reactions between carbons and NaOH and KOH: An insight into the chemical activation mechanism. *Carbon, 41,* 267–275. DOI 10.1016/S0008-6223(02)00279-8.
42. Lu, C. L., Xu, S. P., Gan, Y. X., Liu, S. Q., Liu, C. H. (2005). Effect of pre-carbonization of petroleum cokes on chemical activation process with KOH. *Carbon, 43,* 2295–2301. DOI 10.1016/j.carbon.2005.04.009.
43. Qiao, W., Yoon, S., Mochida, I. (2006). KOH activation of needle coke to develop activated carbons for high-performance EDLC. *Energy & Fuels, 20,* 1680–1684. DOI 10.1021/ef0503131.
44. Haiyee, Z. A., Saim, N., Said, M., Illias, R. M., Mustapha, W. A. W. et al. (2009). Characterization of cyclodextrin complexes with turmeric oleoresin. *Food Chemistry, 114,* 459–465. DOI 10.1016/j.foodchem.2008.09.072.
45. Mane, V. S., Mall, I. D., Srivastava, V. C. (2007). Use of bagasse fly ash as an adsorbent for the removal of brilliant green dye from aqueous solution. *Dyes and Pigments, 73,* 269–278. DOI 10.1016/j.dyepig.2005.12.006.
46. Hall, K. R., Eagleton, L. C., Acrivos, A., Vermeulen, T. (1966). Pore- and solid-diffusion kinetics in fixed-bed adsorption under constant-pattern conditions. *Industrial & Engineering Chemistry Fundamentals, 5,* 212–223. DOI 10.1021/i160018a011.